NeuroImage 264 (2022) 119715

Contents lists available at ScienceDirect

NeuroImage

journal homepage: www.elsevier.com/locate/neuroimage

The human egomotion network

Ria Maxine Ruehl[a,b,*], Virginia L. Flanagin[a,b,c], Leoni Ophey[b], Theresa Marie Raiser[a,b], Katharina Seiderer[b], Matthias Ertl[d], Julian Conrad[a,b,e], Peter zu Eulenburg[b,c,f]

[a] Department of Neurology, University Hospital Munich, Ludwig-Maximilians-University Munich, Marchionini Str. 15, 81377 Munich, Germany
[b] German Center for Vertigo and Balance Disorders, IFB-LMU, University Hospital Munich, Ludwig-Maximilians-University Munich, Marchionini Str. 15, 81377 Munich, Germany
[c] Graduate School of Systemic Neurosciences, Department of Biology II and Neurobiology, Großhaderner Str. 2, 82151 Planegg-Martinsried, Ludwig-Maximilians-University Munich, Germany
[d] Institute of Psychology and Inselspital, Fabrikstrasse 8, 3012 Bern, University of Bern, Switzerland
[e] Department of Neurology, Theodor-Kutze Ufer 1-3, 68167 Mannheim, Medical Faculty Mannheim, University of Heidelberg, Germany
[f] Institute for Neuroradiology, University Hospital Munich, Marchionini Str. 15, 81377 Munich, Ludwig-Maximilians-University Munich, Germany

ARTICLE INFO

Keywords:
Egomotion
Functional Connectivity
Neuroimaging
Human Area 7a
CSv
PcM/pCi
Uvula
VPS

ABSTRACT

All volitional movement in a three-dimensional space requires multisensory integration, in particular of visual and vestibular signals. Where and how the human brain processes and integrates self-motion signals remains enigmatic. Here, we applied visual and vestibular self-motion stimulation using fast and precise whole-brain neuroimaging to delineate and characterize the entire cortical and subcortical egomotion network in a substantial cohort (n=131). Our results identify a core egomotion network consisting of areas in the cingulate sulcus (CSv, PcM/pCi), the cerebellum (uvula), and the temporo-parietal cortex including area VPS and an unnamed region in the supramarginal gyrus. Based on its cerebral connectivity pattern and anatomical localization, we propose that this region represents the human homologue of macaque area 7a. Whole-brain connectivity and gradient analyses imply an essential role of the connections between the cingulate sulcus and the cerebellar uvula in egomotion perception. This could be via feedback loops involved updating visuo-spatial and vestibular information. The unique functional connectivity patterns of PcM/pCi hint at central role in multisensory integration essential for the perception of self-referential spatial awareness. All cortical egomotion hubs showed modular functional connectivity with other visual, vestibular, somatosensory and higher order motor areas, underlining their mutual function in general sensorimotor integration.

1. Introduction

Visual and vestibular cues are indispensable for the perception of self-motion. This fundamentally multisensory process requires the efficient integration of various modalities spanning from visual to vestibular, somatosensory and motor systems (Bremmer et al., 2016).

The focus of earlier neuroimaging studies was mainly to investigate cortical areas involved in the processing of visual self-motion information using optic flow. Responses were found in several cortical areas, including the cingulate sulcus visual area (CSv) (Cardin and Smith, 2010; Wall and Smith, 2008), middle visual temporal area (hMT) (Cardin and Smith, 2010), medial superior temporal area (MST) (Duffy, 1998; Dukelow et al., 2001), ventral intraparietal area (VIP) (Bremmer et al., 2002), visual posterior sylvian area (VPS) (Cardin and Smith, 2010), lateral intraparietal sulcus (IPS)(Pitzalis et al., 2010), V6 complex (Pitzalis et al., 2006; Pitzalis et al., 2010), precuneate motion area (PcM)(Cardin and Smith, 2010) or posterior cingulate area (pCi) (Pitzalis et al., 2020) and putative area 2v (Cardin and Smith, 2010). Whether these areas also respond to vestibular stimulation and form part of a multimodal self-motion network, however, is unclear. One study (n=9) using galvanic vestibular stimulation (GVS) reported vestibular responses in CSv, MST, STSms, and "weak" responses in VIP, but focused solely on these specific areas (Smith et al., 2012)

Furthermore, the involvement of brainstem- and cerebellar hubs in human self-motion perception has not been investigated yet. In the macaque, the cerebellar uvula and nodulus were proposed as key regions for egomotion-processing (Angelaki et al., 2010). Their pivotal role in vestibular processing is evidenced by the amount of vestibular projections reaching the uvula and nodulus via primary vestibular afferents from the otolith organs and semicircular canals and secondary

* Corresponding author at: Department of Neurology, University Hospital Munich, Ludwig-Maximilians-Universitat Munchen, Marchioninistraße 15, 81377 Munich, Germany.
E-mail address: maxine.ruehl@med.uni-muenchen.de (R.M. Ruehl).

https://doi.org/10.1016/j.neuroimage.2022.119715.
Received 25 July 2022; Received in revised form 18 October 2022; Accepted 25 October 2022

afferents from the vestibular nuclei and inferior olive (Barmack et al., 1993; Ono et al., 2000; Ruigrok, 2003). Moreover, in humans a function in optokinetic eye movements could be shown (Ruehl et al., 2017). Also, lesions of the uvula and nodulus impair the ability of perceiving visual motion direction on a noisy background and result in higher perceptual thresholds for head motion (Dahlem et al., 2016; Händel et al., 2009).

Here, we systematically investigated the human egomotion network using visual and vestibular stimulation in a whole brain high-resolution neuroimaging approach in a large cohort (n=131). We strived to delineate multimodal hubs of this network on the supra- and infratentorial level by their responses to visual egomotion compatible stimulation with galvanic stimulation in three different conditions – eyes open while fixating a dot, eyes open in darkness and eyes closed. In a unique multimodal approach, we further characterized the network by means of functional connectivity, connectopic mapping, and correlation with nuclear imaging derived estimates.

2. Methods

2.1. Participants

131 healthy volunteers (70 female,61 male, mean age 26.4 years, range: 23-35 years) were recruited. The participants were divided in three cohorts. 46 participants (23 female, 23 male) took part in the visual stimulation experiment and the galvanic vestibular stimulation (GVS) experiment with eyes open (cohort 1), 42 (21 female, 21 male) in the GVS experiment with eyes open in darkness (cohort 2) and 43 (22 female, 21 male) in the GVS experiment with eyes closed (cohort 3; for detailed description of the experiments see Section 2.3). All participants gave their informed written consent. We determined the modified laterality quotient of handedness and footedness using the 14-item inventory of the Edinburgh test (Chapman and Chapman, 1987). All participants were right-handed, with normal vision, without a previous history of neurotological or ocular motor disorder and without regular medication. The study was carried out in accordance with the Declaration of Helsinki (2013) and was approved by the local ethics committee. Participants were paid for participation. The guidelines and principles for reporting fMRI studies were followed (Poldrack et al., 2008).

2.2. fMRI experiments

The experiment was conducted in a 3 Tesla MRI scanner (Skyra, Siemens, Germany, 64-channel array head/neck coil) using echo-planar imaging (EPI) with a T2* weighted gradient-echo sequence (TR= 700 ms, multi-band factor 6, 54 continuous axial slices covering the entire brain, 2.5 mm isotropic voxels, field of view (FoV) 210 mm^2, TE= 33 ms). resting state data using the identical multi-band EPI-sequence (600 volumes) was obtained prior to the fMRI task sessions with participants fixating the dot in the identical setting. A high-resolution T1-weighted MPrage sequence in sagittal orientation was acquired (TR = 2060 ms \ TE = 2.17 ms, flip angle = 12 deg., FoV = 240 mm^2, slice thickness = 0.8 mm, A-P phase encoding, 0.8 mm isotropic voxels, GRAPPA factor 2).

For the projection of the visual stimuli, a monitor positioned behind the participants' head and an adjustable mirror box reflecting the patterns attached to the head coil at a viewing distance of 16 cm (FoV 30°x18,85°) were used. Eye movements were recorded with an infrared VOG unit (MRI-compatible camera, MRC systems,www.mrc-systems.de). The scanner room and tunnel were darkened. Participants wore earplugs and an inflatable head-cushion (Crania adult Pearltec, Switzerland).

2.3. Tasks and stimuli

The fMRI experiments consisted of two visual stimulation conditions, egomotion compatible (EC) and egomotion incompatible (EIC), and three GVS sessions (eyes open, eyes open in darkness and eyes closed). In the visual stimulation and GVS with eyes open sessions, a randomized block design with a visual rest condition varying in length (see below) was used, with participants fixating a dot in the center of the screen.

The EC stimulus was a high contrast, single optic flow patch consisting of 360 light dots moving on a black background (Fig. 1). The dots were moving coherently around a center with a continuously present fixation dot with either an rotation pattern in clockwise or counterclockwise direction, or an expansion or contraction pattern similar as the stimulus used by Wall and Smith (Wall and Smith, 2008). For the EIC stimulation, nine optic flow patches equal in size and distributed across the visual field were shown, which each contained the identical motion profile as the EC stimulus. Both stimuli were shown in a randomized order alternating with visual rest conditions varying in block-length (block length of visual stimulus 10 TR (7s), 20 repetitions for each condition, visual rest condition 10-19 TR (7-13.3s), 1005 volumes (11.73 min)). All conditions contained a fixation dot positioned in the middle of the screen. A functional localizer was used to delineate response in area MST (Huk et al., 2002).

GVS was conducted via bimastoidal electrodes using a custom-made stimulator with sinusoidal stimuli (0.875Hz, 3mA) after local anaesthesia of the postauricular region (Rühl et al., 2017) (block length 10 TR (7s), 12 repetitions for each condition, rest condition 13-23 TR (9.1-16.1s) 1013 volumes, (11.82 minutes)). The stimulation profile was identical in the three different GVS sessions (eyes open, eyes open in darkness, eyes closed). In the group receiving both visual and vestibular stimulation, the stimuli were presented in a randomized order with a minimal time interval between both tasks of at least 30 minutes. All participants were rating the egomotion-intensity using a standardized questionnaire, where egomotion intensity had to be rated on a scale from 0 (no egomotion at all) to 10 (strong egomotion perception).

2.4. Data analysis for the task-based fMRI sessions

The statistical analysis was performed using SPM12 (Version 7487, Wellcome Department of Cognitive Neurology, London, UK) running on Matlab release 2018b (MathWorks, Natick, MA). The realigned images were stereotactically normalized into the standard anatomical space defined by the Montreal Neurological Institute (MNI) template by means of the DARTEL algorithm including geodesic shooting using an existing MNI-template (http://nist.mni.mcgill.ca/?p=904) and the CAT12 toolbox (version 1450) (Ashburner, 2007). Images were smoothed with an isotropic 4 mm Gaussian kernel. Realignment parameters and a high-pass filter (128 s) were integrated into the design matrix. Statistical parametric maps (SPMs) were generated on a voxel-by-voxel basis with a hemodynamic model of the stimulation periods present during the session (Friston et al., 1995). Single subject t-contrasts were computed for each stimulation condition compared to the respective rest condition. The condition images were entered into a second-level statistical analysis. For the participants of the visual stimulation and GVS experiments with eyes open, a one-way ANOVA was performed. In a between-subject approach, two-sample t-tests using linear t-contrasts were used to compare the different GVS conditions (eyes open while fixating, eyes open in darkness, eyes closed) with the contrast EC>EIC. A conjunction analysis between the contrast EC>EIC and the respective GVS condition in the three different cohorts was performed. Activation maps were considered significant at cluster level at $p<0.001$ (TFCE, FDR corrected, E=0.5) after 10 000 permutations (Smith and Nichols, 2009). When applicable, cytoarchitectonic maps were used for the localization of results (Eickhoff et al., 2005). All results were visualized using *MRIcroG*L (https://www.mccauslandcenter.sc.edu/mricrogl/).

2.5. Data analysis of eye tracking videos

Eye movement videos from the visual motion experiment, in the form of uncompressed AVIs, were collected via the Arrington Re-

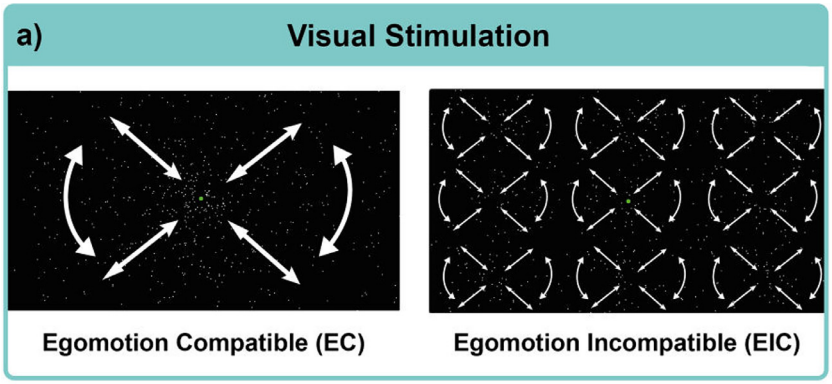

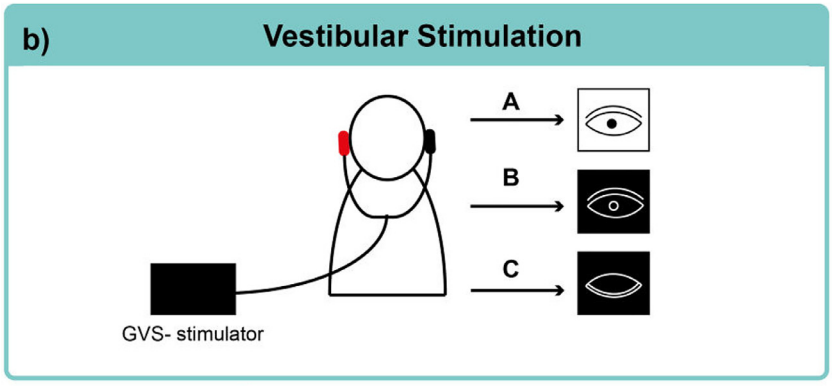

Fig. 1. Experimental Design. (a) Left: Visual egomotion compatible stimulus (EC, left) with a single optic flow patch consisting of 360 white dots on a black background, either rotating in a clockwise/counterclockwise direction or expanding or contracting, similar as the stimulus used by Wall and Smith. (Wall and Smith, 2008). Right: Egomotion incompatible stimulation (EIC, right) with nine optic flow patches equal in size and distributed across the visual field, each containing the identical motion profile as the egomotion compatible stimulus. (b) Galvanic vestibular stimulation (GVS) was applied via electrodes on each mastoid using a sinusoidal (0.875Hz) stimulation pattern (3mA) either with eyes open while fixating a dot (A, cohort 1), with eyes open in darkness (B, cohort 2), or with eyes closed (C, cohort 3) .

search Software (http://www.arringtonresearch.com/; width = 320 px, height = 240 px and 60 Hz). In addition to the AVI-file, a text file containing the timestamps of each video frame and the start of each volume from the functional MRI run were collected to synchronize the video with the functional data. A five-point calibration video was collected to convert the eye position to mm. The videos were cut to the length of the fMRI sequence and converted to the file type required for further analysis with the EyeSeeCam software (revision r3497, Jul. 15 2016). The resulting eye position data was saved together with the frames for each condition and analyzed with Matlab (version 2018b). Blinks were removed from the eye-tracking data by setting the time points from 50 ms before to 50 ms after the blink to NaNs. The data were then linear interpolated and low-pass filtered with a gaussian low-pass filter and cut-off frequency of 20 Hz. Saccades were detected and the variability of eye position in the periods between saccades was used as a measure of eye stability during fixation. Differences in saccade rate and fixation stability between the two conditions were then tested with a paired Wilcoxon signed-rank test with a corrected alpha for multiple comparisons of $\alpha = 0.025$.

2.6. Data analysis for functional connectivty

The ROIs were defined using the regions delineated in the task-experiments (threshold TFCE FDR p<0.001) for a functional connectivity (FC) analysis. The analysis was performed with the resting state (RS)fMRI data and the task-data of all sessions using the CONN toolbox (version 18b; Whitfield-Gabrieli and Nieto-Castanon, 2012; http://www.nitrc.org/projects/conn) for Matlab (version 2019a). First level covariates were employed in the default setting by the CONN Toolbox. Nuisance regressors' time series of white matter (WM) and cerebrospinal fluid (CSF) for denoising and a temporal band-pass filter (0.008-0.09 Hz) and were six principal temporal components of the movement parameters used. The onsets and durations for all task blocks were entered similarly to the SPM12-based GLM approach to analyze the ROI-to-ROI network structure for the different tasks including the rest task separately and to investigate differences in network structure for the tasks compared to the rest condition. All results were thresholded at p<0.05 (FWE corrected, TFCE) after 5000 permutations for the non-parametric thresholding.

2.7. Cross-modal correlation with nuclear imaging derived estimates

Spatial associations between the distribution of specific receptor systems of nuclear imaging derives estimates and our fMRI data including the resting state-FC maps and task-based FC maps of the different ROIs (CSv, PcM/pCi, VPS, h7a, uvula) were calculated using the JuSpace Toolbox (Dukart et al., 2021).

2.8. Connectopic mapping

Using the previously defined ROIs, we examined the connectopic mapping of all egomotion hubs- CSv, PcM/pCi, h7a, VPS (left and right separately) and the uvula with the Congrads toolbox (https://github.com/koenhaak/congrads.git) (Haak et al., 2018) and fslpython (Python version 3.7). Spatial model parameters were tested for significance using PALM (Permutation Analysis of Linear Models) with a threshold of p<0.05 (FWE) after 10 000 permutations (Winkler et al., 2014).

3. Results

3.1. Task-based analysis

Responses specific to egomotion compatible were defined by the contrast EC>EIC and were found in the visual cortex (area V1, V2, V6) and bilaterally in all egomotion hubs (CSv, PcM/pCi, h7a, VPS, uvula). Additional responses were shown in left OP3, area Id7 bilaterally, and in right area 6mc including the supplementary eye field (SEF). Infratentorial responses included the uvula, nodulus and vermal lobule VI (Fig. 2,

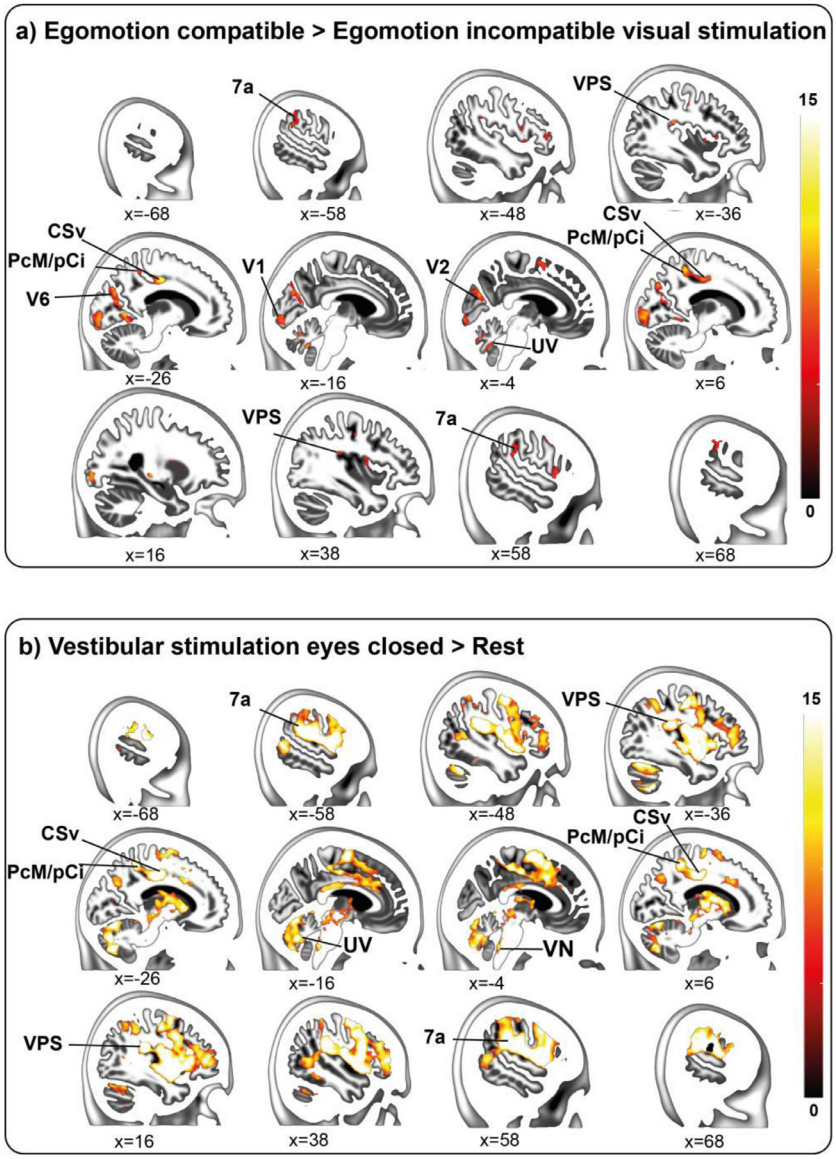

Fig. 2. Responses to visual egomotion stimulation and vestibular stimulation. (a) Specific responses to egomotion compatible stimulation (contrast EC >EIC) gave strong temporo-parietal responses in h7a, VPS and in the visual cortex (V1, V2, V6) as well as in CSv and PcM/pCi (activation maps of cohort 1, n=46). (b) GVS with eyes closed led to responses in the entire egomotion network, including 7a,VPS, CSv, PcM/pCi and the uvula (activation maps of cohort 3, n=43). The color scales on the right of a) and b) depict z-scores. All activation maps were thresholded at p<0.001 TFCE (FDR).

Suppl.Table S1). No differences in eye-movements between the two conditions were found (see Suppl. Fig. 1). Responses in 2v,3av, MT+, MST, and VIP (including mainly responses in the parts pVIP#1, but also lateral parts of pVIP#3 and pVIP#2) (Field et al., 2020; Foster et al., 2021) were seen in the contrast egomotion compatible stimulation>rest, but also during egomotion incompatible stimulation and are thus not specific for visual egomotion perception.

Vestibular stimulation gave responses in all egomotion hubs, the insula and parietal operculum (OP1-4), area hIP1/3, middle temporal gyrus anterior to MST, paracingulate gyrus (including preSMA, SEF), anterior cingulate gyrus, putamen, thalamus, the mesencephalon, vestibular nuclei bilaterally, and the cerebellar vermis with uvula/nodulus, and HIV-VI, Crus I, HVIIIa (Fig. 2, Suppl.Table S1).

3.2. Conjunction analysis

In the conjunction analysis of EC>EIC and GVS with eyes closed, common responses were localized in the uvula, CSv,PcM/pCi, h7a and VPS bilaterally. Smaller cluster included the right SMA (SEF), the right precentral gyrus, right putamen and area 44 bilaterally. Infratentorial responses included the uvula, lobule VIIb and HVI bilaterally (Fig. 3). The results of the conjunction EC>EIC and GVS with eyes open in darkness gave similar results to the conjunction EC>EIC and GVS with eyes closed.

In the conjunction with GVS eyes open additional responses with regards to GVS with eyes closed were found along the parieto-occipital sulcus (peaks in V1, V2, V3d,V3,V6), the anterior insula and the thalamus bilaterally.

3.3. Psychophysical results and correlation analysis with fMRI data

All participants perceived egomotion during the EC task. In the GVS session with eyes open (n=46), the participants perceived egomotion with a mean intensity of 6.13 (SD 1.99; scale 0-10, 0= no egomotion perception, 10 = strong egomotion perception), and in the GVS session with eyes closed (n=43), with a mean intensity of 5.84 (SD 1.87). Correlating the perceived motion intensity during EC and GVS with the task-based fMRI data did not give significant results.

3.4. Results of the analysis of the eye tracking videos

No significant differences were found in the fixation stability (as measured by the variability of eye position) (z = 0.6376, p = 0.5237, Wilcoxon signed-rank test) or the rate of saccades (z = 0.7287,

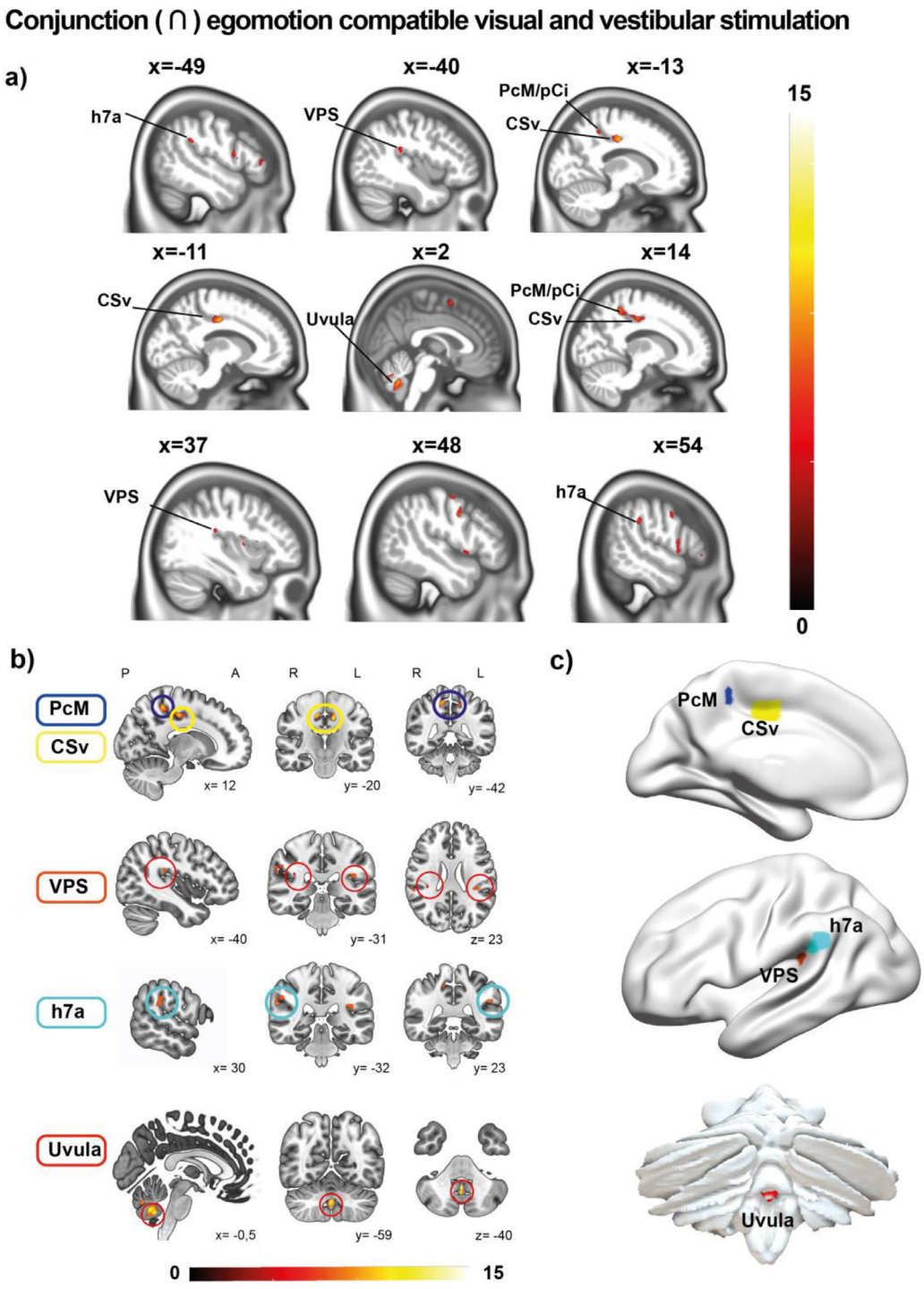

Fig. 3. The human egomotion network. Overview of the results of the conjunction analysis defining the human egomotion network (EC>EIC and GVS with eyes closed) with the central five egomotion core hubs. (a) Sagittal slice view of the results of the conjunction analysis with visual egomotion compatible stimulation (EC>EIC) and vestibular stimulation with eyes closed. Signal increased bilaterally in the temporoparietal cortex in human 7a and VPS, in the cingulate sulcus and gyrus in CSv and PcM/pCI and in the uvula of the cerebellum. (b) Overview of the localization of the five central hubs in sagittal, coronar and axial view of the egomotion network seen, including PcM/pCi (blue) and CSv (yellow) in the cingulate sulcus, the uvula (red) in the cerebellum and area VPS (orange) and h7a (light blue) in the temporal lobe. For better illustration, the ROIs of the egomotion hubs were overlayed. The color scales in a) and b) depict z-scores. All activation maps were thresholded at p<0.001 TFCE (FDR). (c) Overlay of the ROIs of the egomotion hubs (PcM/pCi (blue), CSv (yellow), VPS (orange), h7a (light blue), uvula (red)) on a cortical and infratentorial surface view.

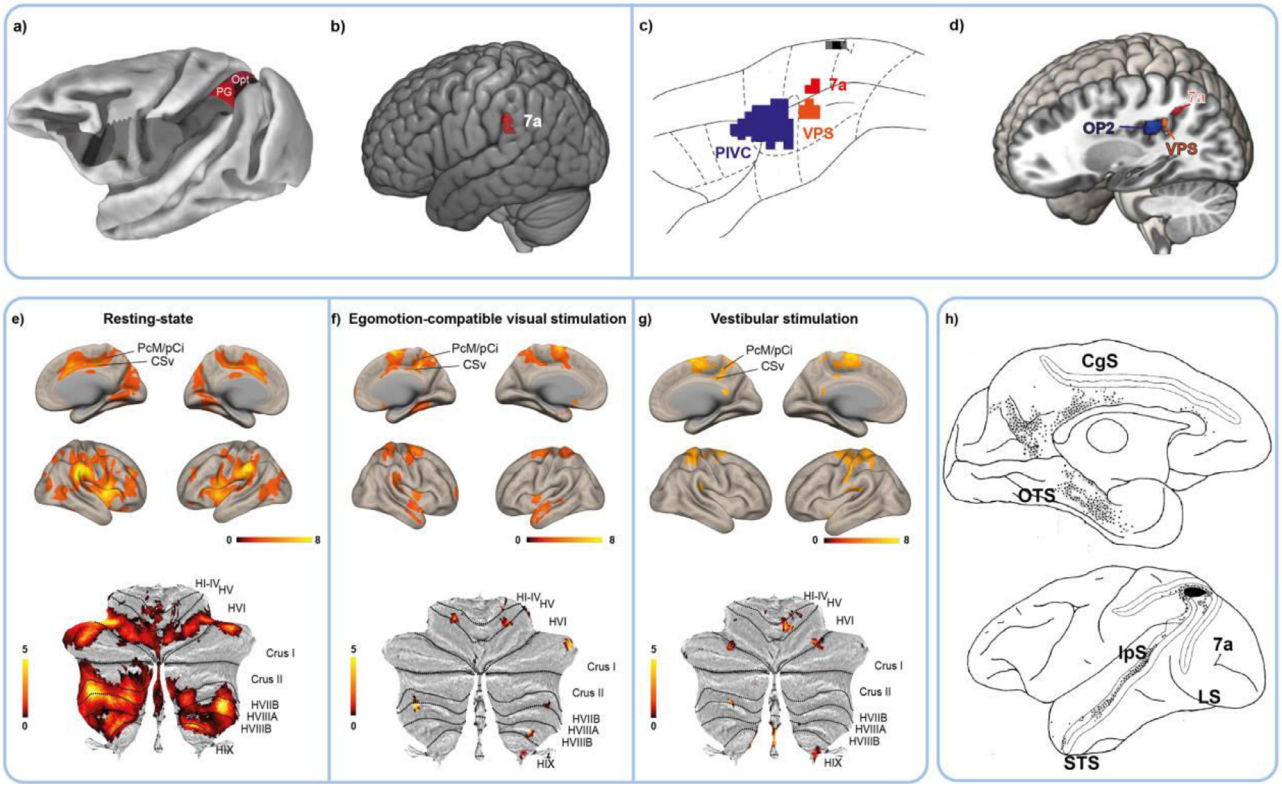

Fig. 4. Localization and functional connectivity of area h7a in comparison to macaque 7a. Overview and comparison of the localization a)-d) and the functional connectivity e)-h) of macaque and human 7a. (a) Schematic drawing of the possible cytoarchitectonical correlates of area 7a, PG and Opt (red), in the macaque (adapted from (Margulies and Petrides, 2013)). (b) Responses in the supramarginal gyrus of the conjunction analysis egomotion compatible visual stimulation and GVS with eyes closed in putative human area 7a. (c) Localization of cortical vestibular areas PIVC, VPS and 7 as shown in the squirrel monkey by Guldin and Grüsser (adapted from(Guldin and Grüsser, 1998)). (d) Multimodal egomotion responses in putative human VPS and human area 7a in relation to OP2 overlapping with the results in nonhuman primates as shown in c). (e) H7a showed RS-FC with all cortical egomotion hubs, with visual (-motion) areas, multisensory areas (pVIP#1 (Foster et al., 2021), hPEc) and leg-representation areas hPE and S1leg (Pitzalis et al., 2019), the premotor cortex bilaterally and the parietal operculum including vestibular core area OP2. In the cerebellum,bottom section) functional connections were found with lobule VI, VIIa, VIII, IX (cerebellar tonsil) and Crus II bilaterally. (f) During visual egomotion stimulation, FC increased bilaterally with CSv, PcM/pCi, the ipsilateral frontal eye field (FEF),SEF bilaterally, pre-SMA, and bilateral cluster in the precuneus, where reaching related responses were localized (Filimon et al., 2007). Right h7a gave additional FC increases in left OP2. In the cerebellum (bottom row) FC increased in left Crus II, right VIIIa, lobule VI bilaterally and in the cerebellar tonsil. (g) During vestibular stimulation, FC increased bilaterally in area CSv,right PcM/pCi, vestibular area OP2 and infratentorial vestibular regions (uvula, right cerebellar tonsil) as well as cerebellar lobule VIII, Crus I and lobule HVI bilaterally. All functional connectivity maps were thresholded at $p<0.001$ TFCE (FWE). The colour scales represent TFCE values. (h) Results of the tracer study by Cavada et al. showing parts of the connections of area 7a in the macaque. These results overlap well with FC maps of h7a (e)-g)), including in the cingulate gyrus (below the cingulate sulcus, CgS), above the occipitotemporal sulcus (OTS), in the upper bank of the superior temporal sulcus (STS) including the superior polysensory area and visual motion areas and in the dorsal prelunate gyrus (figure adapted from (Cavada and Goldman-Rakic, 1989))

$p = 0.4662$) when comparing egomotion compatible and egomotion incompatible stimulation blocks. (Suppl. Fig. 1).

3.5. Functional connectivity analysis

The detailed results of the FC analysis are described in the supplementary information.

3.5.1. Resting state (RS) and task-based functional connectivity of h7a

H7a showed FC with all cortical egomotion hubs, with visual (-motion) areas (V1, V2, V3A, V4, V6,MT/V5, parts of MST) and multisensory areas VIP (visual part pVIP#1) (Field et al., 2020; Foster et al., 2021) and hPEc (Breveglieri et al., 2007), leg-representation areas hPE and S1leg (Pitzalis et al., 2019) (the localization of pVIP, hPEc and S1leg was defined by the coordinates given in (Breveglieri et al., 2007; Field et al., 2020; Foster et al., 2021; Pitzalis et al., 2019), the premotor cortex bilaterally (area 6d2, SEF) and the parietal operculum including vestibular core area OP2.

During egomotion compatible visual stimulation, both h7a showed a stronger FC bilaterally with CSv, PcM/pCi, the ipsilateral frontal eye field (FEF), SEF bilaterally, pre-SMA, and bilateral cluster in the precuneus, where reaching related responses were localized (Filimon et al., 2007). Right h7a gave additional FC increases in left OP2. During vestibular stimulation, both h7a showed FC increases with infratentorial vestibular regions (uvula, right cerebellar tonsil) and right h7a bilaterally in area CSv, vestibular areas OP2 and the nodulus, and the amygdala (Fig. 4).

3.5.2. Resting state and task-based functional connectivity of the uvula

The uvula gave FC with the vermis and vestibulo-cerebellar hubs (flocculi,tonsils), the vestibular nuclei, the oculomotor nucleus, the left parabrachial complex and left locus coeruleus. These connections with arousal/autonomic-function brainstem-hubs are in line with animal literature showing an involvement of the cerebellar vermis with cardiovascular control (Bradley et al., 1991; Samuels and Szabadi, 2008). On the cortical level, no RS-FC was found with any of the egomotion hubs, however, FC increased with right OP2, bilaterally with visual areas (V1, V3v) and the left amygdala.

During egomotion compatible visual stimulation, FC increased bilaterally with CSv, PcM/pCi, visual areas (V1,2,V3v,V3A, V6),FEF

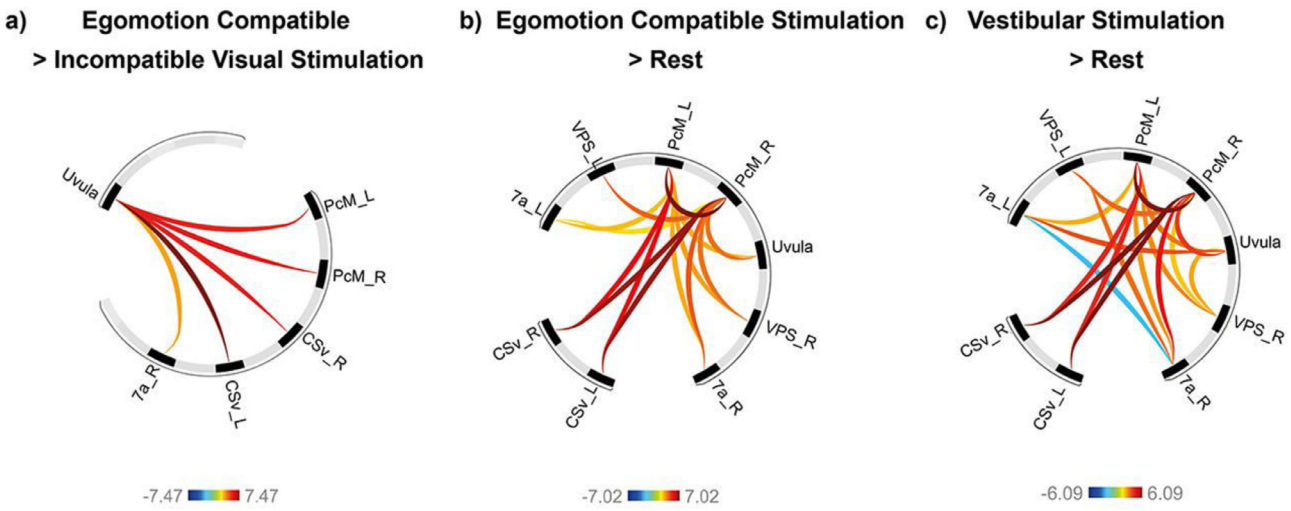

Fig. 5. ROI-to-ROI functional connectivity maps for the egomotion network. (a) Egomotion specific visual stimulation (EC>EIC) resulted in FC increases between the uvula and PcM/pCi, CSv and right 7a bilaterally, pointing at the central role of the cortical-infratentorial between the uvula and the cingulate sulcus axis during visual egomotion perception. (b) Egomotion compatible stimulation contrasted with the rest condition and c) vestibular stimulation resulted in FC increases between PcM/pCi bilaterally and all other egomotion hubs, suggesting a unique role of PcM/pCi as multimodal integration hub. All ROI-to-ROI connections were thresholded at p<0.001 TFCE (FWE). The colour scales represent TFCE values.

and vestibulo-cerebellar areas (flocculi,nodulus). Vestibular stimulation gave FC increases with PcM/pCi and CSv bilaterally, visual areas (V3d, V3A, right V6, right dorsal hMT+), the amygdala and the cerebellar vermis (lobule VIIb, VIIIb,nodulus).

3.5.3. Resting state and task-based functional connectivity of CSv

CSv gave the strongest FC with the uvula, followed by vestibulo-cerebellar hubs (flocculi, cerebellar tonsils), and the vestibular nuclei. CSv showed cortical FC with all egomotion hubs, the parietal operculum (OP1, OP2, OP4,OP8), cingulate eye field (CEF), SEF, FEF, visual areas (V1, V2,V3A, V4, hMT+, V6) and with the supplementary motor area (SMA), preSMA and motor-integration areas (hPEc, hPE) (Pitzalis et al., 2019).

During egomotion compatible visual stimulation, FC increased with PcM/pCi, contralateral CSv and the uvula, all eye fields (FEF, CEF (Ruehl et al., 2021), SEF, ipsilateral parietal eye field (PEF)), visual areas (V1, V3d, V3A, V6 bilaterally) and a cluster posteriorly adjacent to OP2. Right CSv additionally gave FC with the hippocampus bilaterally, and right OP2. During GVS, FC of CSv increased with PcM/pCi, right h7a, uvula,SEF, hippocampus and amygdala bilaterally. Left CSv gave additional increases with right VPS, left OP1 and OP2.

3.6. Resting state and task-based functional connectivity of PcM/pCi

PcM/pCi gave FC with the contralateral PcM/pCi, CSv bilaterally, and h7a. FC increased with visual areas (V1,V2, V3A, V6), the SMA, pre-SMA, SEF, CEF and visuo-motor integration areas (hPEc, HPE) (Pitzalis et al., 2019), the parietal operculum (OP1, OP2, OP4,OP8), ipsilateral parahippocampal gyrus, hippocampus, and with vestibulo-cerebellar areas (flocculi, cerebellar tonsils).

Egomotion compatible visual stimulation gave FC increases with the contralateral area PcM/pCi, CSv, h7a, and VPS. FC further increased with visual areas (V1- V6), eye fields (FEF, SEF, ipsilateral CEF), SMA/pre-SMA, the parietal operculum with vestibular core area OP2, OP1, and the hippocampus bilaterally, and the ipsilateral amygdala and flocculus. Vestibular stimulation led to increased FC with CSv bilaterally, ipsilateral h7a, the uvula, vestibular area OP2 bilaterally, right OP1, anterior ipsilateral MST and SEF.

3.6.1. Resting state functional connectivity of VPS (aPIC)

Human VPS showed FC bilaterally with all egomotion hubs, visual areas (V3A,MT/V5), areas OP1,3,4, vestibular area OP2, CEF, SMA, pre-SMA, the hippocampus and amygdala.

During egomotion compatible visual stimulation, FC increased between the contralateral VPS, contralateral PcM/pCi and h7a and with visual areas (V1 bilaterally, contralateral V2, V3d, V6), SMA, SEF bilaterally, and contralateral HVIIIa. Vestibular stimulation did not lead to FC increases of area VPS.

3.6.2. ROI-to-ROI functional connectivity maps of the egomotion network

The contrast EC > EIC gave increased FC between the uvula and PcM/pCi, CSv and right h7a (Fig. 5). The contrast EC > rest showed bilateral signal increases between PcM/pCi and all ROIs, apart from left VPS, which showed increased FC only with right PcM/pCi. During GVS, FC increased bilaterally between PcM/pCi and CSv, the uvula, right VPS and right 7a, as well as in-between both areas PcM/pCi, and right PcM/pCi and left VPS. Furthermore, FC increased between the uvula and left h7a, left VPS and right h7a, but decreased between both h7a (Fig. 5).

3.6.3. Cross-modal correlation with nuclear imaging derived estimates

A correlation of the FC maps of the different cortical egomotion hubs with serotonoergic- (5HT1a,-b,2a) GABAa-, opioid- (MU), and noradrenaline (NAT) receptor maps was found during RS. Task-based FC maps showed during EC a common correlation of all hubs with serotonergic (5HT1b, 5Ht2a) and GABAa receptors, whereas during GVS, common correlations were found for serotonergic (5HT1b) and NAT receptors (Suppl. Fig. 2).

3.6.4. Connectopic mapping

Connectopic analysis of the cerebellar uvula revealed a significant gradient (Fig. 6c) with a predominantly posterior-to-anterior direction. The analysis of mean connectopy of the uvula with both areas CSv gave a similar pattern (Fig. 6d). CSv depicted a mirrored anterior-to-posterior and lateral-to-medial axis in its gradient composition (Fig. 6a). The nature of these gradients (e.g. somatotopy of body motion components, derivatives of head motion velocities or trajectories) is unclear at this point. For all other egomotion hubs, no significant gradient structure was identified.

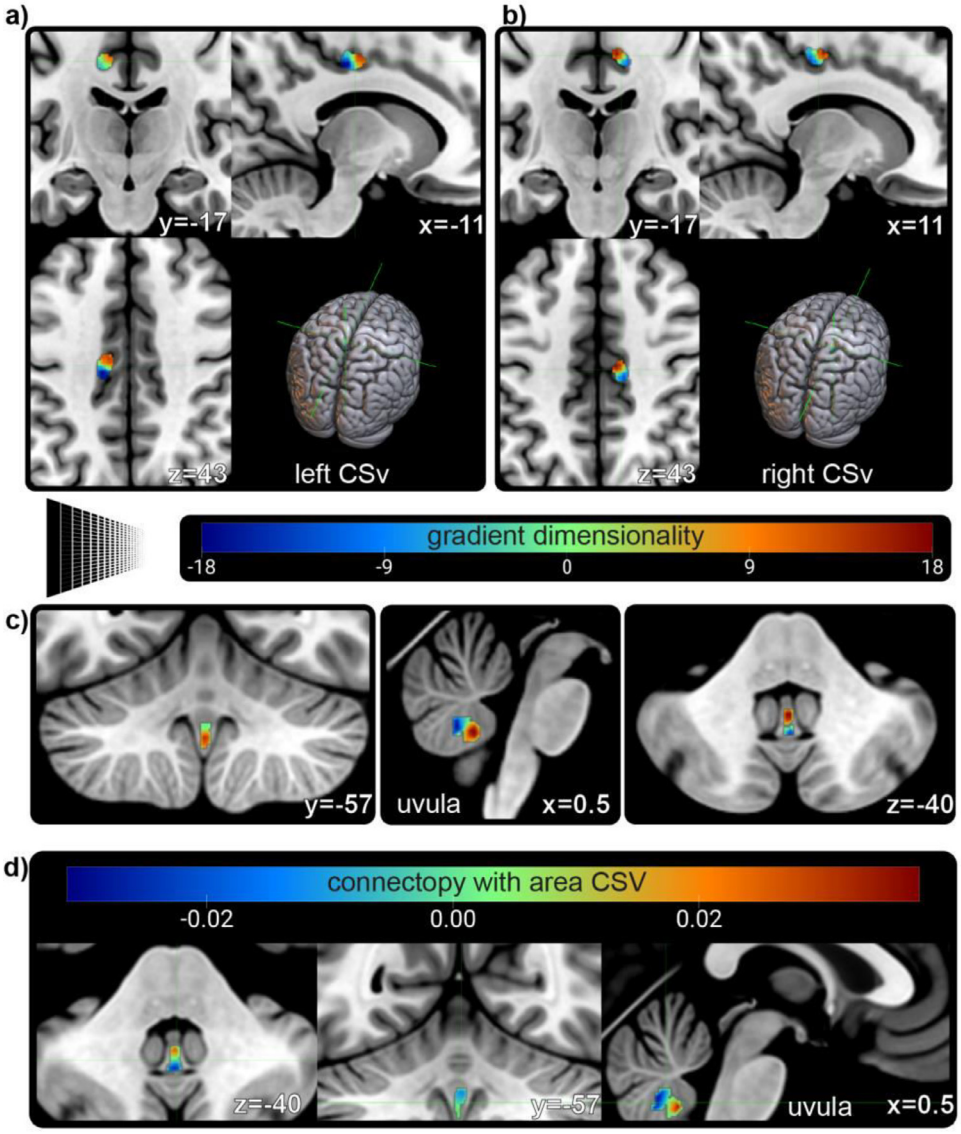

Fig. 6. Gradients within the main egomotion hubs. (a) Depiction of the significant gradient found within the left area CSv using connectopic mapping with all other brain regions. The main axis runs anterior-to-posterior and lateral-to-medial. The detect spatial pattern appears to be bipolar with a small transition zone (green). The units of the gradient dimensionality scale are arbitrary. The scale also applies to b) and c). (b) The spatial connectivity pattern of the right area CSv robustly mirrors its homotopic partner region in its gradient characterisation and orientation. (c) The cerebellar uvula was found to contain a significant anterior-to-posterior gradient in the connectopic group analysis. The underlying nature of the gradient (e.g. somatotopic representation, head velocity or directional derivatives) remains to be investigated. (d) Mean connectivity pattern of the uvula with both CSv areas was found to resemble a spatial arrangement similar to the detected general gradient in c).

4. Discussion

Our results reveal five egomotion core hubs: area CSv, PcM/pCi, VPS, a region in cytoarchitectonic areas PF/PFcm, representing the human correlate of macaques' area 7a, and the cerebellar uvula (Fig. 3). The individual FC patterns highlight the multimodal interconnections of these hubs with visual, vestibular, somatosensory and (ocular-) motor-regions. Our results suggest a common neurotransmitter basis of all hubs and significant gradients exclusively in the uvula and CSv. Functional connections of all cortical egomotion hubs with the SMA and pre-SMA underline their involvement in motor planning (Serra et al., 2019).

Our data point at CSv as a central multisensory interface for processing egomotion information, particularly in the presence of visual cues. Our task-based and functional connectivity-results thereby complement the previously reported function of CSv in optic flow, ocular-motor and vestibular processing (Ruehl et al., 2021; Smith et al., 2012; Wall and Smith, 2008). Contrasting with earlier works, we found clear evidence for functional connectivity with primary visual- and visual motion areas (V1, V3A, V6). These could represent pathways for passing visual input to area CSv (Smith et al., 2018), which then might feed visual sensory and oculomotor information in the egomotion network. The functional connectivity pattern of CSv switched during GVS away from visual-motion areas to egomotion areas, SEF and OP2, supporting a role of CSv as an essential mediating hub between visual perception, (ocular-) motor, and vestibular/navigation related areas.

Especially the functional connections between the cingulate sulcus (CSv, PcM/pCi) and the uvula seem to play an essential role in visual egomotion perception. The connections with CSv/PcM might reflect cortico-cerebellar loops involved in a continuous updating of multimodal egomotion information to coordinate visuo-spatial signals and higher order motor behaviour. The significant role of CSv and the uvula within the egomotion network is further substantiated by their unique connectopic fingerprint, contrasting with other egomotion hubs.

Our results suggest the uvula as the cerebellar egomotion core region, extending evidence from nonhuman-primates to humans (Angelaki et al., 2010) and an earlier report of altered self-motion perception in patients with chronic midline cerebellar degeneration (Bertolini et al., 2012). Via its multimodal functional connections, the uvula could provide unconscious vestibular egomotion information to cortical hubs via feedback loops.

The signal increases in vicinity to CSv correspond to area PcM/pCi (Cardin and Smith, 2010; Cardin and Smith, 2011; Pitzalis et al., 2020). Its responses to egomotion compatible optic flow stimuli, voluntary head- (Schindler and Bartels, 2018) and leg-movements (Serra et al., 2019) suggest a role in sensorimotor integration and locomotion guiding. Our findings of strong multimodal responses and its unique func-

tional connections with all egomotion hubs make PcM/pCI an ideal candidate for multimodal integration and self-referential spatial awareness (Parvizi et al., 2021). Being located at the border of the cingulate sulcus/precuneus and the functional connected to the temporo-parietal junction, PcM/pCi could be involved in spatial encoding of the pooled visual and vestibular information provided by other egomotion hubs. PcM/pCi was the only hub showing increased bilateral connectivity to vestibular region OP2 during both stimulation modalities. These connections might feed egomotion related signals to the vestibular core area (zu Eulenburg et al., 2012). FC increases with the hippocampus during visual egomotion stimulation further support a role in egocentric memory processing and spatial updating as previously hypothesized (Land, 2014; Schindler and Bartels, 2018). Interestingly, functional connectivity increases with the hippocampus were also found in area CSv and h7a. To examine their role in spatial memory processing could be the aim of future studies.

Multimodal responses to egomotion stimulation were found bilaterally in the supramarginal gyrus. We propose that this region corresponds to macaque area 7a, which has not been identified in humans so far (Amiez and Petrides, 2009; Siegel and Read, 1997b) (Figs. 3-4).

Macaque 7a is located between the superior temporal and intraparietal sulcus (Merchant et al., 2001; Siegel and Read, 1997a), and has been synonymously termed cytoarchitectonic area PG (Rozzi et al., 2006; Siegel and Read, 1997a; von Bonin, 1947). A recent study however functionally localized macaque 7a in the more caudal part Opt of the inferior parietal lobule (Cottereau et al., 2017) (Fig. 4). Comparative architectonic observations proposed the human homologue of area PG in the angular gyrus (Margulies and Petrides, 2013). Our data suggest that human area 7a (h7a) is localized in the anterior division of the supramarginal gyrus, covering parts of cytoarchitectonic areas PFcm and PF. Macaque 7a responds to optic flow and vestibular stimulation, whereby a vestibular predominance in self-motion processing with only a smaller part of neurons involved in multisensory processing has been shown (Avila et al., 2018; Siegel and Read, 1997a). This is in line with our findings of larger activation cluster and higher t-values in h7a during vestibular stimulation (Suppl. Fig. 3), and missing FC increases with visual areas during EC stimulation.

A recent motion-platform-study in humans demonstrated a strong modulation of activity in an area in the supramarginal gyrus during egomotion, possibly representing h7a. Responses here depended on the congruency of head- and eye-position or translational motion direction (Ertl et al., 2021). Interestingly, also in macaque 7a responses are modulated by the eye- and head-position, suggesting a role in constructing a "world-centered" representation of space and guidance of motor action (Siegel and Read, 1997a; Snyder et al., 1998). Furthermore, the results of our FC analysis overlap strongly with the results of animal tracer studies of area 7a (Akbarian et al., 1988; Cavada and Goldman-Rakic, 1989; Neal et al., 1990; Rozzi et al., 2006) (Fig. 4), substantiating our hypothesis. In particular its resting-state and task-based functional connectivity with vestibular core region OP2 signal an embedment in the vestibular network and are in line with tracer studies in the squirrel and java monkey showing strong cortical inputs of 7a to PIVC (Akbarian et al., 1988). Our results further suggest a role of h7a in coordinating egomotion signals for limb-movement preparation and motor-planning to guide motor behavior and locomotion, as task-based FC increases were found with pre-motor areas, the eye-fields, an area in the anterior precuneus related to reaching responses (Filimon et al., 2007) and with visuo-motor integration area PEc (Pitzalis et al., 2019).

Human area VPS (anterior posterior insular cortex, aPIC) (Billington and Smith, 2015; Frank et al., 2014; Sunaert et al., 1999) was the fifth hub found to respond to multimodal egomotion stimulation. Previously shown responses to vestibular stimulation, voluntary head motion and voluntary leg movements suggested a role in multimodal sensory integration (Frank et al., 2016; Schindler and Bartels, 2018; Serra et al., 2019). The responses in VPS, OP2 and h7a during vestibular stimulation are perfectly in line with data of the squirrel monkey, where VPS has been localized posterior to the vestibular core area PIVC, and anterior to area 7a (Guldin and Grüsser, 1998). These findings further substantiate our localization of the human area 7a and the proposed role of area OP2 as human homologue for area PIVC (Raiser et al., 2020; zu Eulenburg et al., 2012). The FC pattern indicates a predominant involvement of VPS during visual egomotion perception, with FC increases with visual areas (V3A,MT/V5), h7a and PcM/pCI. (Fig. 4).

No visual egomotion-specific responses were found in MST and VIP, as both areas responded during egomotion compatible and incompatible stimulation. Recent findings in animals proposed that vestibular signals might facilitate motion processing in MSTd neurons by enhancing the separability of tuning profiles (Sasaki et al., 2017). This might explain the vestibular responses in MST, which could serve to differentiate object-motion from self-motion, but not contribute essentially to self-motion perception. The lack of responses specific to visual egomotion processing in VIP is in line with a recent study suggesting a primary function of VIP in object-motion processing (Field et al., 2020). Our results support the view of VIP and MST as parts of a motion detection system (Foster et al., 2021), but without exclusive responses to egomotion stimulation.

Our findings of a common correlation of the task-based FC maps of all hubs with serotonergic (5HT1b, 5Ht2a) and $GABA_A$ receptors during EC stimulation correspond with data showing direct effects of 5-HT agonists on visual processing in animals (Michaiel et al., 2019) and a correlation of $GABA_A$ receptor binding potential and visual cortex activity in humans (Qin et al., 2012). The correlations during GVS with 5HT1b and NAT receptors are in line with animal data showing noradrenergic and serotonergic responses in the vestibular nuclei complex (Cransac et al., 1996; Licata et al., 1993). Our data suggest that these neurotransmitters play a role during vestibular induced egomotion perception, however, the neurotransmitter architecture of the cortical vestibular network has not been investigated so far.

5. Conclusion

In summary, our results show a human egomotion network spanning from cortical areas in the cingulate sulcus (Csv, PcM/pCi) and temporoparietal cortex (VPS, h7a) to the cerebellum (uvula) with a common neurotransmitter basis and multisensory functional connections. Visual egomotion perception seems to involve particularly the cortico-cerebellar axis between the cingulate sulcus and the uvula. The outstanding role of CSv and the uvula within this network is further substantiated by their unique connectopic gradient. Our data support the hypothesis of a central function of area PcM/pCi as multimodal integrator essential for the perception of self-referential spatial awareness.

6. Data and code availability statement

We used publicly available software. Group results can be uploaded to neurovault/openneuro. Single subject data access is not available due to german privacy laws and limited consent at the time of the study.

Declaration of Competing Interest

None.

Credit authorship contribution statement

Ria Maxine Ruehl: Conceptualization, Data curation, Formal analysis, Investigation, Methodology, Project administration, Resources, Software, Validation, Visualization, Writing – original draft, Writing – review & editing. **Virginia L. Flanagin:** Formal analysis, Methodology, Resources, Software, Writing – review & editing. **Leoni Ophey:** Data curation, Investigation, Resources. **Theresa Marie Raiser:** Data curation,

Investigation, Resources. **Katharina Seiderer:** Data curation, Investigation, Resources. **Matthias Ertl:** Methodology. **Julian Conrad:** Data curation, Investigation, Resources. **Peter zu Eulenburg:** Conceptualization, Formal analysis, Methodology, Project administration, Resources, Supervision, Validation, Writing – review & editing.

Acknowledgements

This work was supported by the German Federal Ministry of Education and Research (BMBF 01 EO 0901). We would like to thank Thomas Eggert for his thoughtful insights into the eye-tracking analysis and his saccade detection algorithm.

Supplementary materials

Supplementary material associated with this article can be found, in the online version, at doi:10.1016/j.neuroimage.2022.119715.

References

Akbarian, S., Berndl, K., Grüsser, O.J., Guldin, W., Pause, M., Schreiter, U., 1988. Responses of single neurons in the parietoinsular vestibular cortex of primates. Ann. N Y Acad. Sci. 545, 187–202.
Amiez, C., Petrides, M., 2009. Anatomical organization of the eye fields in the human and non-human primate frontal cortex. Prog. Neurobiol. 89, 220–230.
Angelaki, D.E., Yakusheva, T.A., Green, A.M., Dickman, J.D., Blazquez, P.M., 2010. Computation of egomotion in the macaque cerebellar vermis. Cerebellum 9, 174–182.
Ashburner, J., 2007. A fast diffeomorphic image registration algorithm. Neuroimage 38, 95–113.
Avila, E., Lakshminarasimhan, K.J., DeAngelis, G.C., Angelaki, D.E., 2018. Visual and vestibular selectivity for self-motion in macaque posterior parietal area 7a. Cereb. Cortex 29, 3932–3947.
Barmack, N.H., Baughman, R.W., Errico, P., Shojaku, H., 1993. Vestibular primary afferent projection to the cerebellum of the rabbit. J. Comp. Neurol. 327, 521–534.
Bertolini, G., Ramat, S., Bockisch, C.J., Marti, S., Straumann, D., Palla, A., 2012. Is vestibular self-motion perception controlled by the velocity storage? Insights from patients with chronic degeneration of the vestibulo-cerebellum. PLoS One 7, e36763.
Billington, J., Smith, A.T., 2015. Neural mechanisms for discounting head-roll-induced retinal motion. J. Neuroscience 35, 4851–4856.
Bradley, D.J., Ghelarducci, B., Spyer, K.M., 1991. The role of the posterior cerebellar vermis in cardiovascular control. Neurosci. Res. 12, 45–56.
Bremmer, F., Klam, F., Duhamel, J.R., Ben Hamed, S., Graf, W., 2002. Visual-vestibular interactive responses in the macaque ventral intraparietal area (VIP). Eur. J. Neurosci. 16, 1569–1586.
Bremmer, F., Smith, A., Cuturi, L., Kaliuzhna, M., Blanke, O., Macneilage, P., Churan, J., Frank, S., Greenlee, M., 2016. Multisensory integration in self motion perception. Multisensory Res. 29.
Breveglieri, R., Galletti, C., Monaco, S., Fattori, P., 2007. Visual, somatosensory, and bimodal activities in the macaque parietal area PEc. Cereb. Cortex 18, 806–816.
Cardin, V., Smith, A.T., 2010. Sensitivity of human visual and vestibular cortical regions to egomotion-compatible visual stimulation. Cereb. Cortex 20, 1964–1973.
Cardin, V., Smith, A.T., 2011. Sensitivity of human visual cortical area V6 to stereoscopic depth gradients associated with self-motion. J. Neurophysiol. 106, 1240.
Cavada, C., Goldman-Rakic, P.S., 1989. Posterior parietal cortex in rhesus monkey: I. Parcellation of areas based on distinctive limbic and sensory corticocortical connections. J. Comp. Neurol. 287, 393–421.
Chapman, L.J., Chapman, J.P., 1987. The measurement of handedness. Brain Cogn. 6, 175–183.
Cottereau, B.R., Smith, A.T., Rima, S., Fize, D., Héjja-Brichard, Y., Renaud, L., Lejards, C., Vayssière, N., Trotter, Y., Durand, J.B., 2017. Processing of egomotion-consistent optic flow in the Rhesus macaque cortex. Cereb. Cortex 27, 330–343.
Cransac, H., Cottet-Emard, J.M., Pequignot, J.M., Peyrin, L., 1996. Monoamines (norepinephrine, dopamine, serotonin) in the rat medial vestibular nucleus: endogenous levels and turnover. J. Neural Transm. (Vienna) 103, 391–401.
Dahlem, K., Valko, Y., Schmahmann, J.D., Lewis, R.F., 2016. Cerebellar contributions to self-motion perception: evidence from patients with congenital cerebellar agenesis. J. Neurophysiol. 115, 2280–2285.
Duffy, C.J., 1998. MST neurons respond to optic flow and translational movement. J. Neurophysiol. 80, 1816–1827.
Dukart, J., Holiga, S., Rullmann, M., Lanzenberger, R., Hawkins, P.C.T., Mehta, M.A., Hesse, S., Barthel, H., Sabri, O., Jech, R., Eickhoff, S.B., 2021. JuSpace: a tool for spatial correlation analyses of magnetic resonance imaging data with nuclear imaging derived neurotransmitter maps. Hum. Brain Mapp. 42, 555–566.
Dukelow, S.P., DeSouza, J.F., Culham, J.C., van den Berg, A.V., Menon, R.S., Vilis, T., 2001. Distinguishing subregions of the human MT+ complex using visual fields and pursuit eye movements. J. Neurophysiol. 86, 1991–2000.
Eickhoff, S.B., Stephan, K.E., Mohlberg, H., Grefkes, C., Fink, G.R., Amunts, K., Zilles, K., 2005. A new SPM toolbox for combining probabilistic cytoarchitectonic maps and functional imaging data. Neuroimage 25, 1325–1335.
Ertl, M., Zu Eulenburg, P., Woller, M., Dieterich, M., 2021. The role of delta and theta oscillations during ego-motion in healthy adult volunteers. Exp. Brain Res. 239, 1073–1083.
Field, D.T., Biagi, N., Inman, L.A., 2020. The role of the ventral intraparietal area (VIP/pVIP) in the perception of object-motion and self-motion. Neuroimage 213, 116679.
Filimon, F., Nelson, J.D., Hagler, D.J., Sereno, M.I., 2007. Human cortical representations for reaching: mirror neurons for execution, observation, and imagery. Neuroimage 37, 1315–1328.
Foster, C., Sheng, W.-A., Heed, T., Ben Hamed, S., 2021. The macaque ventral intraparietal area has expanded into three homologue human parietal areas. Progr. Neurobiol. 209, 102185.
Frank, S.M., Baumann, O., Mattingley, J.B., Greenlee, M.W., 2014. Vestibular and visual responses in human posterior insular cortex. J. Neurophysiol. 112, 2481–2491.
Frank, S.M., Wirth, A.M., Greenlee, M.W., 2016. Visual-vestibular processing in the human Sylvian fissure. J. Neurophysiol. 116, 263–271.
Friston, K.J., Frith, C., Turner, R., Frackowiak, R.S.J., 1995. Characterizing evoked hemodynamics with fMRI. Neuroimage 2, 157–165.
Guldin, W.O., Grüsser, O.J., 1998. Is there a vestibular cortex? Trends Neurosci. 21, 254–259.
Haak, K.V., Marquand, A.F., Beckmann, C.F., 2018. Connectopic mapping with resting-state fMRI. Neuroimage 170, 83–94.
Händel, B., Thier, P., Haarmeier, T., 2009. Visual motion perception deficits due to cerebellar lesions are paralleled by specific changes in cerebro-cortical activity. J. Neuroscience 29, 15126–15133.
Huk, A.C., Dougherty, R.F., Heeger, D.J., 2002. Retinotopy and functional subdivision of human areas MT and MST. J. Neuroscience 22, 7195–7205.
Land, M.F., 2014. Do we have an internal model of the outside world? Philos. Trans. R. Soc. Lond. B Biol. Sci. 369, 20130045.
Licata, F., Li Volsi, G., Maugeri, G., Ciranna, L., Santangelo, F., 1993. Effects of noradrenaline on the firing rate of vestibular neurons. Neuroscience 53, 149–158.
Margulies, D.S., Petrides, M., 2013. Distinct parietal and temporal connectivity profiles of ventrolateral frontal areas involved in language production. J. Neuroscience 33, 16846–16852.
Merchant, H., Battaglia-Mayer, A., Georgopoulos, A.P., 2001. Effects of optic flow in motor cortex and area 7a. J. Neurophysiol. 86, 1937–1954.
Michael, A.M., Parker, P.R.L., Niell, C.M., 2019. A hallucinogenic serotonin-2A receptor agonist reduces visual response gain and alters temporal dynamics in mouse V1. Cell Rep. 26, 3475–3483 e3474.
Neal, J.W., Pearson, R.C.A., Powell, T.P.S., 1990. The connections of area PG, 7a, with cortex in the parietal, occipital and temporal lobes of the monkey. Brain Res. 532, 249–264.
Ono, S., Kushiro, K., Zakir, M., Meng, H., Sato, H., Uchino, Y., 2000. Properties of utricular and saccular nerve-activated vestibulocerebellar neurons in cats. Exp. Brain Res. 134, 1–8.
Parvizi, J., Braga, R.M., Kucyi, A., Veit, M.J., Pinheiro-Chagas, P., Perry, C., Sava-Segal, C., Zeineh, M., Staalduinen, E.K.V., Henderson, J.M., Markert, M., 2021. Altered sense of self during seizures in the posteromedial cortex. Proc. Natl. Acad. Sci. 118, e2100522118.
Pitzalis, S., Galletti, C., Huang, R.-S., Patria, F., Committeri, G., Galati, G., Fattori, P., Sereno, M.I., 2006. Wide-field retinotopy defines human cortical visual area V6. J. Neuroscience 26, 7962–7973.
Pitzalis, S., Sereno, M.I., Committeri, G., Fattori, P., Galati, G., Patria, F., Galletti, C., 2010. Human v6: the medial motion area. Cereb. Cortex 20, 411–424.
Pitzalis, S., Serra, C., Sulpizio, V., Committeri, G., de Pasquale, F., Fattori, P., Galletti, C., Sepe, R., Galati, G., 2020. Neural bases of self- and object-motion in a naturalistic vision. Hum. Brain Mapp. 41, 1084–1111.
Pitzalis, S., Serra, C., Sulpizio, V., Di Marco, S., Fattori, P., Galati, G., Galletti, C., 2019. A putative human homologue of the macaque area PEc. Neuroimage 202, 116092.
Poldrack, R.A., Fletcher, P.C., Henson, R.N., Worsley, K.J., Brett, M., Nichols, T.E., 2008. Guidelines for reporting an fMRI study. Neuroimage 40, 409–414.
Qin, P., Duncan, N.W., Wiebking, C., Gravel, P., Lyttelton, O., Hayes, D.J., Verhaeghe, J., Kostikov, A., Schirrmacher, R., Reader, A.J., Northoff, G., 2012. GABA(A) receptors in visual and auditory cortex and neural activity changes during basic visual stimulation. Front. Hum. Neurosci. 6, 337.
Raiser, T.M., Flanagin, V.L., Duering, M., van Ombergen, A., Ruehl, R.M., Zu Eulenburg, P., 2020. The human corticocortical vestibular network. Neuroimage 223, 117362.
Rozzi, S., Calzavara, R., Belmalih, A., Borra, E., Gregoriou, G.G., Matelli, M., Luppino, G., 2006. Cortical connections of the inferior parietal cortical convexity of the macaque monkey. Cereb. Cortex 16, 1389–1417.
Ruehl, R.M., Hinkel, C., Bauermann, T., Eulenburg, P.Z., 2017. Delineating function and connectivity of optokinetic hubs in the cerebellum and the brainstem. Brain Struct. Funct. 222, 4163–4185.
Ruehl, R.M., Ophey, L., Ertl, M., zu Eulenburg, P., 2021. The cingulate oculomotor cortex. Cortex 138, 341–355.
Rühl, R.M., Stephan, T., Dieterich, M., Eulenburg, P.z., 2017. P 11 Towards a human vestibular cortex – manifold confounders hamper the delineation of vestibular responses in functional neuroimaging. Clin. Neurophysiol. 128, e331–e332.
Ruigrok, T.J., 2003. Collateralization of climbing and mossy fibers projecting to the nodulus and flocculus of the rat cerebellum. J. Comp. Neurol. 466, 278–298.
Samuels, E.R., Szabadi, E., 2008. Functional neuroanatomy of the noradrenergic locus coeruleus: its roles in the regulation of arousal and autonomic function part I: principles of functional organisation. Curr. Neuropharmacol. 6, 235–253.
Sasaki, R., Angelaki, D.E., DeAngelis, G.C., 2017. Dissociation of self-motion and object motion by linear population decoding that approximates marginalization. J. Neuroscience 37, 11204–11219.

Schindler, A., Bartels, A., 2018. Integration of visual and non-visual self-motion cues during voluntary head movements in the human brain. Neuroimage 172, 597–607.
Serra, C., Galletti, C., Di Marco, S., Fattori, P., Galati, G., Sulpizio, V., Pitzalis, S., 2019. Egomotion-related visual areas respond to active leg movements. Hum. Brain Mapping 40, 3174–3191.
Siegel, R.M., Read, H.L., 1997a. Analysis of optic flow in the monkey parietal area 7a. Cereb. Cortex 7, 327–346.
Siegel, R.M., Read, H.L., 1997b. Construction and representation of visual space in the inferior parietal lobule. In: Rockland, K.S., Kaas, J.H., Peters, A. (Eds.), Extrastriate Cortex in Primates. Springer US, Boston, MA, pp. 499–525.
Smith, A.T., Beer, A.L., Furlan, M., Mars, R.B., 2018. Connectivity of the Cingulate Sulcus Visual Area (CSv) in the Human Cerebral Cortex. Cereb. Cortex 28, 713–725.
Smith, A.T., Wall, M.B., Thilo, K.V., 2012. Vestibular inputs to human motion-sensitive visual cortex. Cereb. Cortex 22, 1068–1077.
Smith, S.M., Nichols, T.E., 2009. Threshold-free cluster enhancement: addressing problems of smoothing, threshold dependence and localisation in cluster inference. Neuroimage 44, 83–98.
Snyder, L.H., Grieve, K.L., Brotchie, P., Andersen, R.A., 1998. Separate body- and world-referenced representations of visual space in parietal cortex. Nature 394, 887–891.
Sunaert, S., Van Hecke, P., Marchal, G., Orban, G.A., 1999. Motion-responsive regions of the human brain. Exp. Brain Res. 127, 355–370.
von Bonin, G., 1947. The neocortex of Macaca mulatta. Monogr. Med. Sci. 5, 136.
Wall, M.B., Smith, A.T., 2008. The representation of egomotion in the human brain. Curr. Biol. 18, 191–194.
Whitfield-Gabrieli, S., Nieto-Castanon, A., 2012. Conn: a functional connectivity toolbox for correlated and anticorrelated brain networks. Brain Connect 2, 125–141.
Winkler, A.M., Ridgway, G.R., Webster, M.A., Smith, S.M., Nichols, T.E., 2014. Permutation inference for the general linear model. Neuroimage 92, 381–397.
Zu-Eulenburg, P., Caspers, S., Roski, C., Eickhoff, S.B., 2012. Meta-analytical definition and functional connectivity of the human vestibular cortex. Neuroimage 60, 162–169.